MNA Beurskens et al.

The role of carbon on the H-mode confinement in ASDEX Upgrade with a metal wall

The role of carbon on the H-mode confinement in ASDEX Upgrade with a metal wall

M.N.A. Beurskens[1,2,*], M.G. Dunne[3], L. Frassinetti[4], M Bernert[3], M. Cavedon[3], R. Fischer[3], A. Järvinen[5], A Kallenbach[3], F. M. Laggner[6], R. M. McDermott[3], G. Tardini[3], E. Viezzer[3], E. Wolfrum[3], the ASDEX Upgrade Team and the EUROfusion MST1 team[†].

[1] *Max-Planck-Institut für Plasmaphysik, D-17491 Greifswald,Germany*
[2] *previously CCFE Fusion Association, Culham Science Centre, Abingdon, OX14 3DB,UK*
[3] *Max-Planck-Institut für Plasmaphysik, D-85748 Garching,Germany*
[4] *Division of Fusion Plasma Physics, Association VR, KTH, Sweden*
[5] *Aalto University, Tekes, P.O.Box 4100, 02015 Espoo, Finland*
[6] *Institute of Applied Physics, TU Wien, Fusion-ÖAW, 1040 Vienna, Austria*

1) Introduction

Future fusion devices such as ITER and DEMO will have plasma facing wall material out of metal. This is because the conventional use of carbon as a first wall material is prohibited due to its high tritium retention properties. It is common to apply a low Z impurity (like nitrogen) as a divertor radiator in metal devices to reduce steady state heat loads to the divertor [1,2,3]. Experiments in those devices have also shown that the energy confinement can be affected by the different plasma impurity composition. It is found in ASDEX Upgrade with a tungsten wall (AUG-W) and JET with an ITER like mixed Be-W wall (JET-ILW) that confinement improvement with N_2 seeding stems from the pedestal region and results in confinement quality previously observed often only in carbon devices [4,5,6,7]. In addition, earlier experiments in JET with a carbon wall (JET-C) show no beneficial of an additional low-Z impurity seeding (N_2 and Ne in this case) on plasma confinement [8].

These observations raise the question whether in carbon devices the presence of intrinsic carbon has an unknown beneficial impact on the confinement, and whether in metal devices a low Z impurity like nitrogen substitutes this role. Initial experiments with carbon seeding (through CD_4 seeding) in AUG-W show a promising confinement improvement [6]. Unfortunately the CD_4-flow was not calibrated and C-impurity concentration measurements were unavailable. For this reason, new experiments in AUG-W have compared the impact of seeding N_2 and CD_4 on plasma confinement. Carbon is usually banned in metal devices, and hence only a low number of plasmas discharges are allowed to be run with carbon seeding in this initial experiment. As the pedestal stability is affected by plasmas shaping and the low-Z impurity seeding is expected to mainly affect the pedestal pressure, the plasma triangularity is also varied during the impurity seeding phase to investigate how the effects of seeding and shaping combine.

In this experiment N_2 and CD_4 were seeded at a level where N_2 seeding had previously shown a confinement benefit. A transition to divertor detachment is avoided due to the possible impact of detachment on confinement [1,2,3]. This paper describes the experimental strategy and global plasma performance in section 2. The impurity concentration and divertor

---

properties such as radiation and detachment state are discussed in section 3. The confinement properties are discussed in section 4 and the paper ends with a discussion in section 5.

2) Experiment description.

In AUG the most extensive N_2 seeding studies aiming at confinement optimisation have been conducted in plasmas with a plasma current of $I_p = 1MA$, $B_T = 2.5T$ at low triangularity ($\delta = 0.2$) and an edge safety factor of $q_{95} = 4.6$ [4]. In this paper, this reference scenario has been selected for comparing the effect of N_2 and deuterated methane (CD_4) seeding on plasma confinement as part of an ongoing wider study [3,7,9] in which the potential of various seeding gases, is reviewed (He, N_2, CD_4, Ne, Ar and Kr). A control experiment comparing N_2 and CD_4 seeding has been conducted with:

1. A reference plasma without seeding – (#30513) – $\Gamma_D \sim 2.5 * 10^{22}$ elec/s,
2. A plasma with N_2 seeding – (#30507) – $\Gamma_D \sim 2.5 * 10^{22}$ elec/s and $\Gamma_N \sim 1 * 10^{22}$ molec./s,
3. A plasma with CD_4 seeding – (#30518) – $\Gamma_D \sim 1.3 * 10^{22}$ elec/s and $\Gamma_{CD4} \sim 1.5 * 10^{22}$ molec./s.

To additionally study the effect of pedestal stability, halfway through the seeding phase the upper triangularity is varied from $\delta_{up} \sim 0.05$ to $\delta_{up} \sim 0.3$, see Figure 1. The lower triangularity is fixed at $\delta_{low} \sim 0.45$ in order not to affect the divertor geometry, which is known to strongly affect pumping capability and recycling properties of the plasma. The CD_4 fuelling and seeding rates have been adjusted such that the total number of electrons from deuterium remains as close as possible to that of the reference plasma as well as a C-rate as close to the N-rate in the N-seeded plasma. However, note that the CD_4 flow rate is not well calibrated and the level of C in the plasma is later verified by Charge Exchange Recombination Spectroscopy (CXRS), and the divertor and main chamber neutral pressure changes are measured by pressure gauges (see Figure 2). The plasma current and magnetic field are set to $I_p/B_T = 1MA/2.5T$, and the total input power $P_{tot} \sim 12MW$ ($P_{NBI} = 10MW$ and $P_{ECRH} = 1.5MW$, $P_{Ohm} = 0.5MW$) is selected in order to reach normalised pressure $\beta_N \sim 1.8$ in the reference plasma as a starting value. Figure 2 shows an overview of relevant signal time traces. The time windows used in this paper for comparison of the low and high triangularity phases are indicated by grey bars in the figure from 3-3.2 s and 5-5.2s subsequently. It should be noted that none of the three shots discussed here suffer from confinement degrading 2/1 or 3/2 MHD activity in the plasma centre.

The impact of the light-impurity seeding on the global plasma parameters is shown in Figure 3. The plasma stored energy W_{MHD} and normalised confinement $H_{98,y2}$ increase by 20-30%, with a similar change for both the N_2 and CD_4 seeded plasmas. The change in triangularity δ_{up} from 0.05 to 0.3 has a beneficial impact on the stored energy for both the unseeded and seeded cases. The plasma density and ELM frequency (Figure 2) remain unaffected by the seeding gasses but are affected by the plasma shaping where the density normalised to the Greenwald density limit increases from $f_{GW} \sim 0.6$ to 0.75 and the ELM frequency decreases from ~140Hz to ~45 Hz. (The individual ELM energy losses increase from ~ 50 kJ to ~150kJ while the product f_{ELM} x $\Delta W_{ELM} \sim$ constant.) Finally the neutral particle inventory is not strongly affected by the seeding of neither N_2 nor CD_4; The neutral particle density in the divertor $n_{0\text{-}divertor}$ and main chamber $n_{n\text{-}main}$ remain largely unaffected as does the divertor compression ratio $n_{0\text{-}divertor}/n_{0\text{-}main} \sim 200\text{-}230$, which is a typical range for AUG.
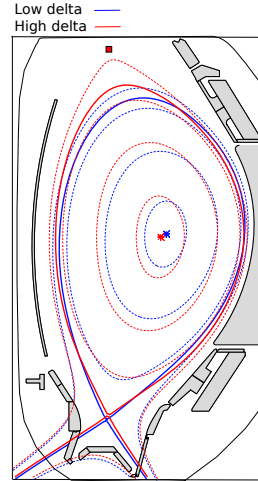
Figure 1: Low and high triangularity configurations used in the N_2 vs CD_4 seeding comparison experiment. The upper triangularity is varied from $\delta_{up} \sim 0.05$ to $\delta_{up} \sim 0.3$ and the lower triangularity is fixed at $\delta_{low} \sim 0.45$
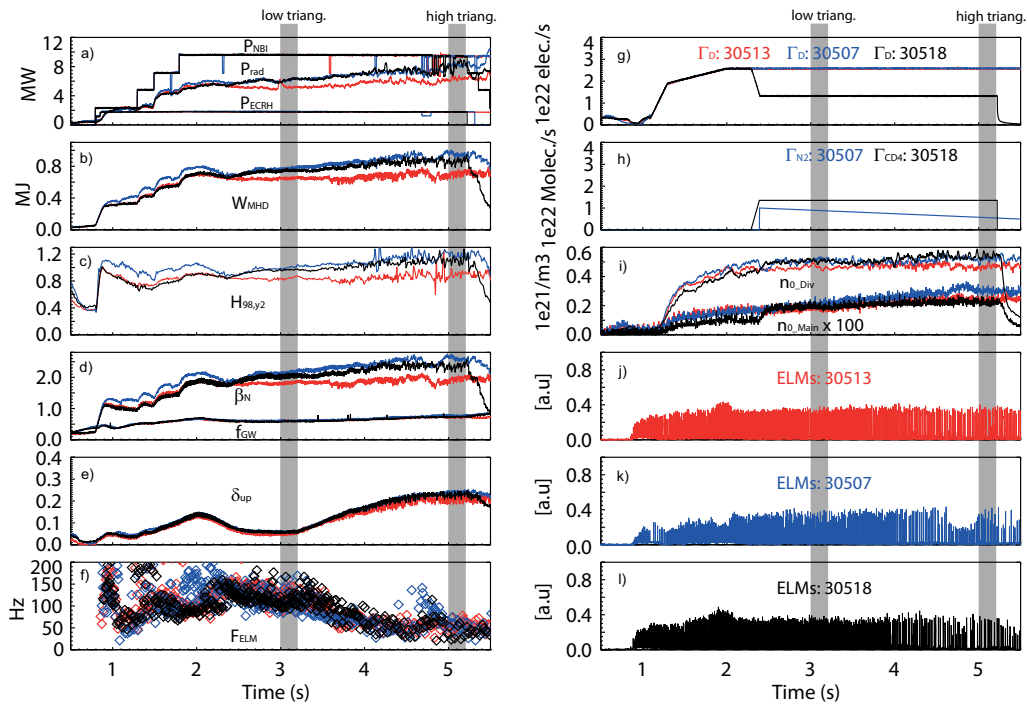
Figure 2: Overview of time traces (the grey bars indicate the time windows used to study the low and high triangularity phases) a) neutral beam and ECRH power and total radiated power; b) total plasma stored energy; c) Normalised confinement $H_{98,y2}$; d) β_N and density normalised to the Greenwald density f_{GW}; e) upper plasma triangularity; f) ELM frequency; g) Deuterium Fuelling level; h) N_2 and CD_4 seeding levels; i) divertor and outer-mid-plane main chamber neutral pressures; j- l) ELM time traces measured by divertor shunt-current

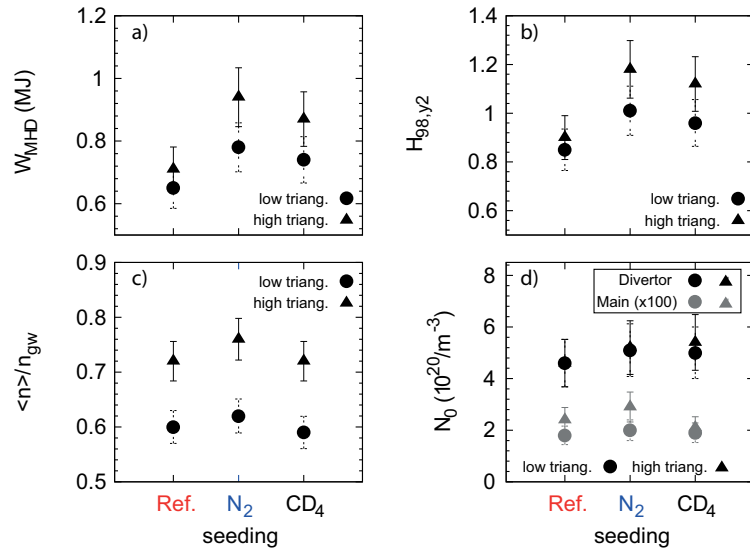*Figure 3: Time averaged parameters for low triangularity phase (t=3-3.2s) and high triangularity phase (t=5-5.2s) for a) plasma stored energy; b) normalised confinement $H_{98,y2}$; c) Greenwald density fraction; d) divertor and outer-mid-plane main chamber neutral pressure*

3) Impurity concentration and divertor conditions

No accurate absolute calibration of CD_4 gas flow was available at the time of the experiment. However, impurity density measurements of the fully stripped N^{7+} and C^{6+} from the core and edge charge exchange diagnostics (CXRS) show that both N_2 and CD_4 seeded plasmas have an impurity concentration of c_{N7+} and c_{C6+} ~1.5-2% going from the plasma centre to the pedestal top region for the low triangularity phase (Figure 4). In the high triangularity phase similar concentrations have been measured, although the match is not perfect. To calculate the profiles of effective charge only the fully stripped ions are taken into account providing a lower estimate of Z_{eff} (including a typical AUG-W baseline concentration of 0.5% B^{4+} – which is not measured.) Due to the similar charge of C^{6+} and N^{7+} the thus derived Z_{eff} profiles rise from 1.3 across the core profile for the unseeded reference plasma to 1.5 to 2 going from the plasma centre to the pedestal top region for both impurity species. Note that for the high triangularity plasmas, although we intended to match c_{N7+} and c_{C6+} the match in Z_{eff} has improved due to the mismatch in c_{N7+} and c_{C6+}.

It is important to note that the edge CXRS data do not have an absolute calibration for the impurity density profiles. Therefore this data is cross calibrated at the point where the edge and core CXRS data meet around $\rho_{pol} \sim 0.9$. Nevertheless, from the cross calibrated profiles it can be seen that both c_{N7+} and c_{C6+} as well as the derived Z_{eff} profile have a pedestal. Previous studies assuming neoclassical transport in the pedestal have shown that also a pedestal in the combined charge impurity profiles can be expected [10]. This is an important observation in investigating the role of ion dilution on the pedestal confinement (more on this in the discussion section 5).

Figure 5 shows that the radiation potential of C and N are very similar. As the separatrix electron temperature is around 100 eV and rises further going inwards, most of the radiation from these light impurities will be outside the last closed flux surface. Figure 6a, shows an

example for the low triangularity CD_4 seeded plasma; the tomographic reconstruction of the AUG bolometer radiation indeed shows that most radiation is outside the separatrix and mainly in the divertor region. The tomographic reconstruction is insightful to qualitatively verify where the radiation takes place. However, for a quantitative comparison in our experiment it is better to look at the direct lines of sight of the lateral bolometer system (white lines in Figure 6a). This data is shown in Figure 6b and c. The N_2 and CD_4 seeded cases are virtually indistinguishable for both triangularities and feature increased divertor radiation compared to the reference plasma.

The seeding increases the total radiation power from a fraction of 50% to 70% of the total input power ($P_{NBI}+P_{ECRH}+P_{Ohm}$), Figure 7a&b. Note that although locally the divertor radiation shows the largest change, integrated over the divertor volume versus the main plasma volume, the divertor and main chamber radiation have increased by similar amounts, Figure 7c. The main chamber radiation is increased due to an increase of the main plasma radiation in central channels 15-35 of the bolometer, see Figure 6. In addition, the main chamber radiation in the high triangularity plasmas is higher than in the low triangularity plasmas, partly due the higher plasma density at increased triangularity, and hence increased Bremsstrahlung radiation ($\sim n^2$). As a result of these two factors, the ratio of divertor versus main chamber radiation remains unchanged when the seeding is introduced and remains at $P_{rad,DIV}/P_{rad,main} \sim 1.8$-2 for the low triangularity plasmas and at $P_{rad,DIV}/P_{rad,main} \sim 1.3$-1.4 for the high triangularity plasmas, Figure 7d.

The increased divertor radiation by the N_2 or CD_4 seeding does not lead to divertor detachment; The outer divertor moves from an attached regime to a regime of high recycling, as can be seen in Figure 8a and b. The Langmuir probe measurements are taken from 50-90% of the ELM cycle (using ELM synchronisation in the 3-3.2 s (low delta) and 5-5.2s (high delta) time windows used). They show a strong increase in the ion saturation current and a slight decrease of the electron temperature for both seeding gasses, typical for a transition to an attached high recycling regime [12].
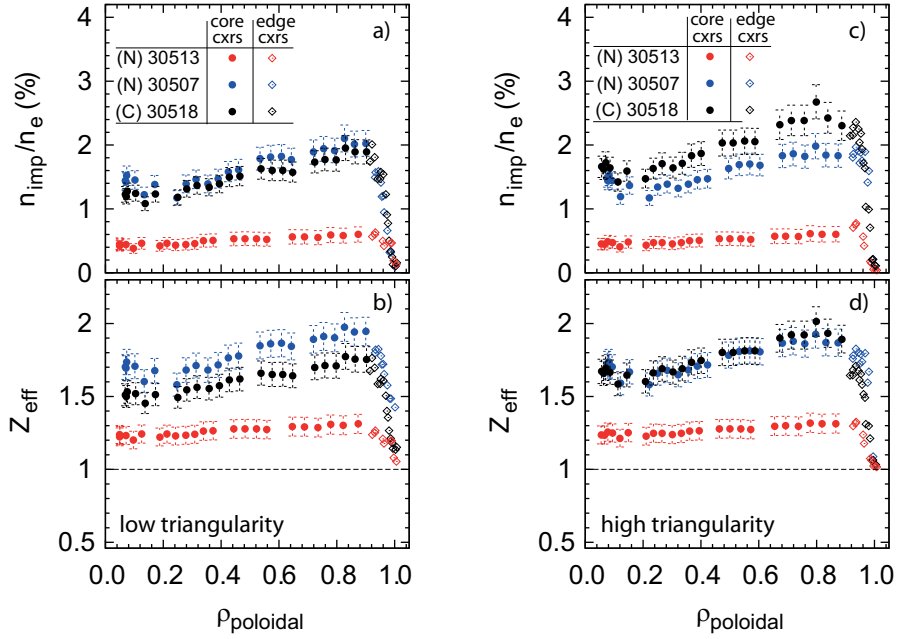
Figure 4: (a) Impurity concentration from core and edge CXRS and (b) derived Z_{eff} of the fully stripped N^{7+} or C^{6+} impurities for the low (t=3-3.2s) and c) and d) for high (t=5-5.2s) triangularity phases of the discharges. The edge CXRS measurements do not have an absolute calibration and have been normalised to the core CXRS measurements at the pedestal top.
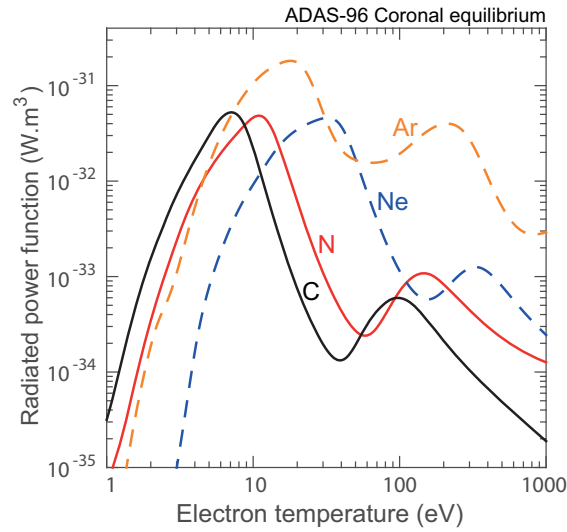

Figure 5: The radiative potential curves for carbon (C, black), and nitrogen (N, red) as a function of the electron temperature. The lines represent coronal equilibrium values calculated using the ADAS 96 database [11]. The curves for Ne and Ar have also been added for comparison in discussion section 5.
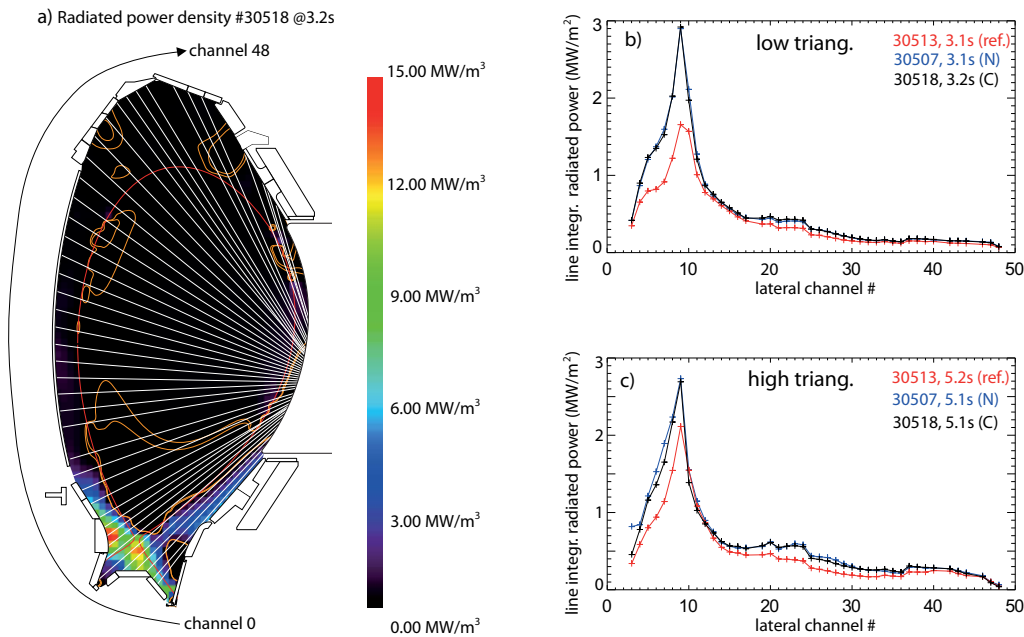
Figure 6 a) Example radiated power density for CD$_4$ seeding, low triangularity phase from tomographic reconstruction using bolometer lines of sights. The impurity radiation is concentrated in the divertor region and below the X-point. The lateral channels and their numbering order used in figures b&c are indicates by the white lines. b) low triangularity and c)high triangulary phase: line integrated radiated power from individual lateral bolometer lines of sights for the reference unseeded (30513), the N$_2$ seeded (30507) and the CD$_4$ seeded (30518) plasmas. The increase in divertor radiation for the seeded cases, peaks around bolometer channel 9
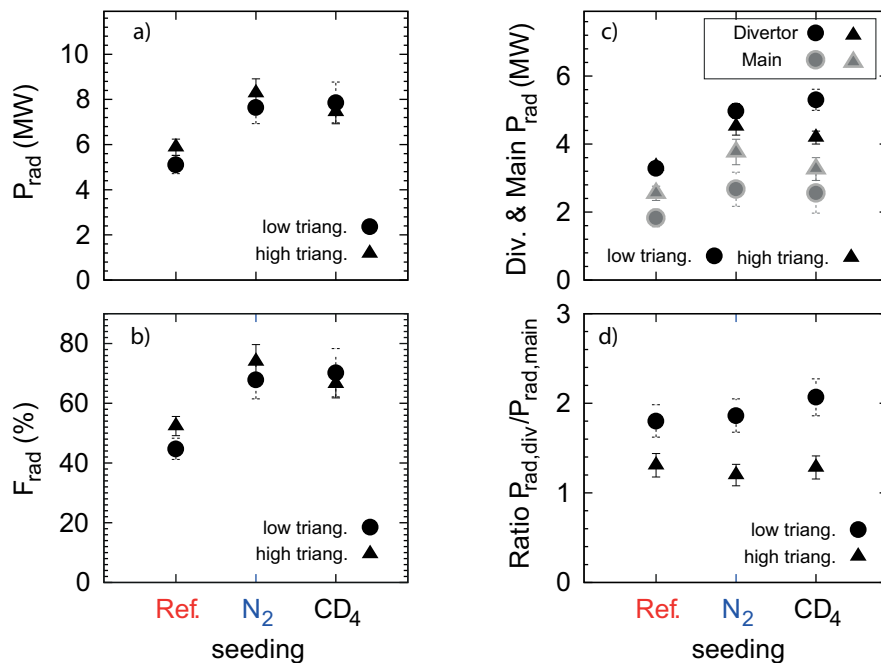

Figure 7 a) Total radiated power as measured by bolometry; b) Total radiation as a fraction of the total input power; c) radiated power split between divertor and main chamber radation; d) ratio of divertor and main chamber radiation.
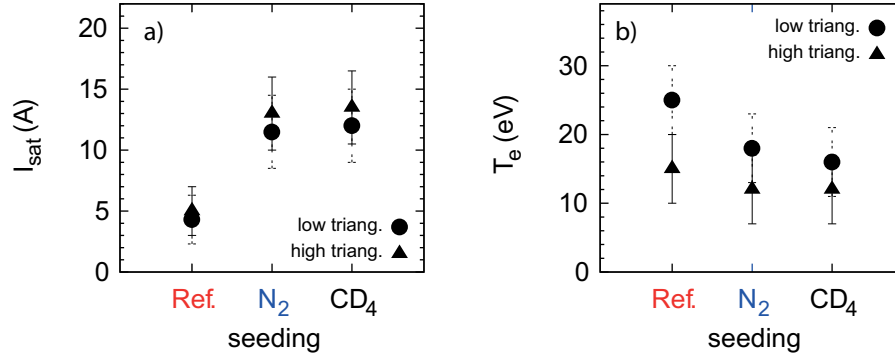
Figure 8 a) ion saturation current and b) target temperature as measured by Langmuir probes taken from 50-90% of the ELM cycle using ELM synchronisation between 3-3.2 s (low delta) and 5-5.2s (high delta)

4) Confinement, pedestal and ELMs

As seen in Figure 3, the global confinement improvement with either N_2 or CD_4 seeding is of the order of 20-30%, which is similar to that reported in N_2 seeded plasmas reported in [4]. Figure 9 shows that for the low and high triangularity plasmas respectively, the main confinement improvement stems from an increase of both ion and electron temperature profiles. The density profiles are relatively unaffected by seeding in both triangularities.

As the core T_e and T_i gradient lengths remain unchanged across the experiment [7], the confinement benefit comes from an increase in the pedestal temperature. As can be seen in Figure 10, both the electron and ion temperature increase by 20-30%, which through core temperature profile stiffness leads to the similar global confinement benefit of either N_2 or CD_4 seeding. While the pedestal density is unchanged with the applied seeding gasses, the triangularity has a large effect on the pedestal density; by changing the upper triangularity from $\delta_{up}\sim0.05$ to $\delta_{up}\sim0.3$ (lower triangularity fixed at $\delta_{low}\sim0.45$), the plasmas pedestal density increases from $6.5\ 10^{19}m^{-3}$ to $9\ 10^{19}m^{-3}$ at constant temperature in both seeded and unseeded plasmas

Various mechanisms have been proposed to explain the confinement benefit of light impurity seeding [6,7,9]. The most likely candidate is a mechanism that provides a beneficial effect on the pedestal stability. The pedestal pressure and pressure gradients in all 6 cases presented here are consistent with peeling ballooning theory as is discussed in [7]. Hence, the impurities provide a beneficial effect to the pedestal which leads to higher pedestal pressure, which in turn leads to a proportionally higher core pressure through core profile stiffness. The subsequent higher global pressure β_N has in its turn a beneficial effect on the pedestal ballooning stability [13] and allows higher pedestal pressure gradients to be sustained. This interplay between core and edge can intuitively be well understood, and is likely to be at the root of the underlying physics of confinement improvement with impurity seeding. However, the mechanism that leads to an improved pedestal pressure has so-far not been identified. This will be further discussed in section 5. An indication that the pedestal conditions have changed is also given by a change in the ELM collapse dynamics. Figure 2 shows that the ELM frequency is unaffected by seeding N_2 and CD_4, however the ELM collapse speed has indeed changed for both seeding gasses compared to the reference plasmas. In [14,15] it was shown that the ELM collapse time was significantly reduced when comparing unseeded and

seeded plasmas in AUG and JET. Figure 11. shows that both N_2 and CD_4 seeding influence the ELM collapse times in similar manner.
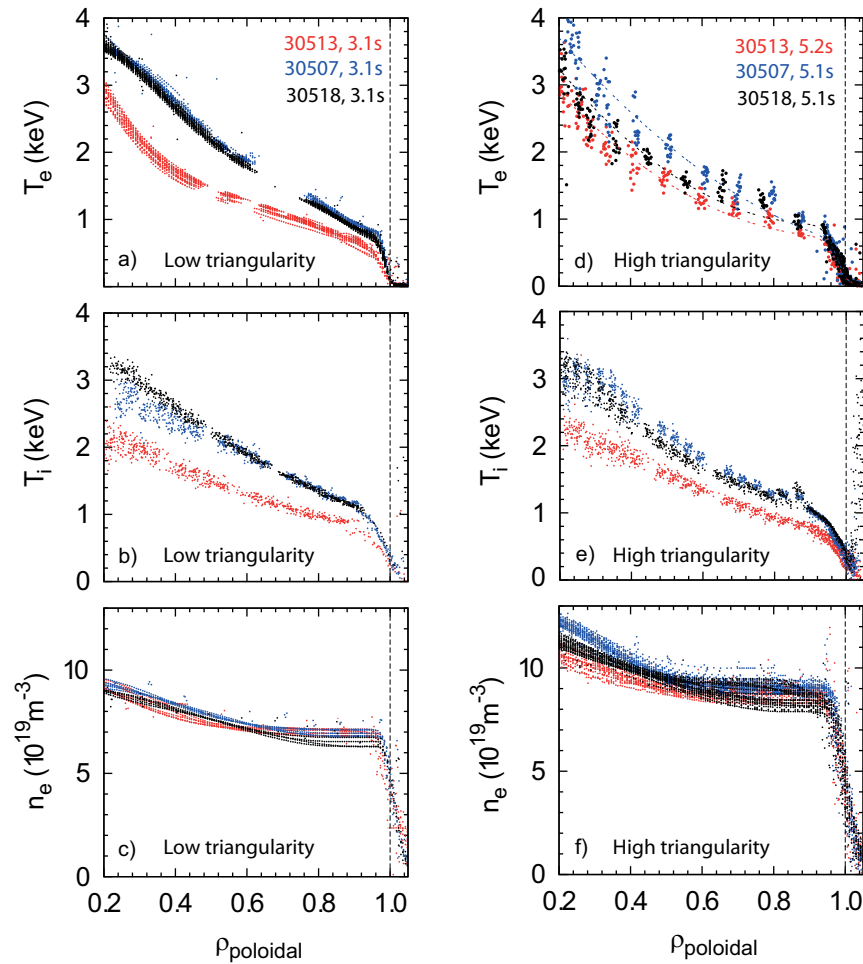

Figure 9: a) Electron temperature from ECE and Thomson scattering, b) ion temperature from core and edge charge exchange spectroscopy and c) electron density from integrated data analysis (Thomson scattering, Lithium beam and interferometry)for the low triangularity phase of the unseeded reference shot (30513) the N_2 seeded (30507) and CD_4 seeded shot (30518).d-f)same as a-c) for the high triangularity phase (note that no ECE was available for the high triangularity phase due the ECE density cut-off).
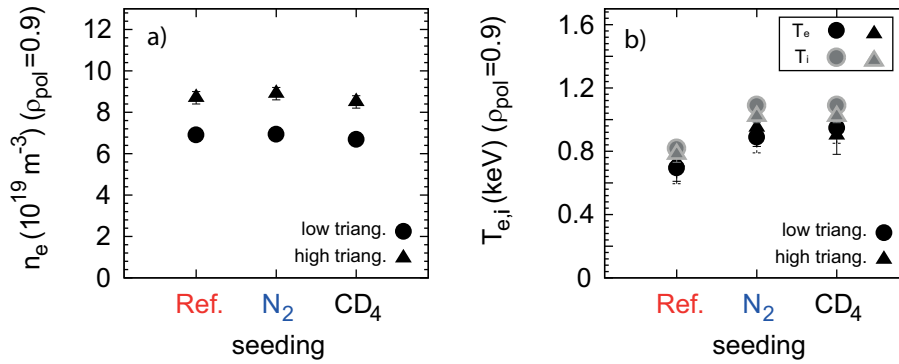
Figure 10 (a) Pedestal electron density and (b)Pedestal electron (black) and ion (grey) temperature at $\rho_{pol}=0.9$ as a measure for the pedestal top values. Shaping affects the pedestal density (a) whereas seeding N_2 or CD_4 lead to an increase in pedestal temperature (b).
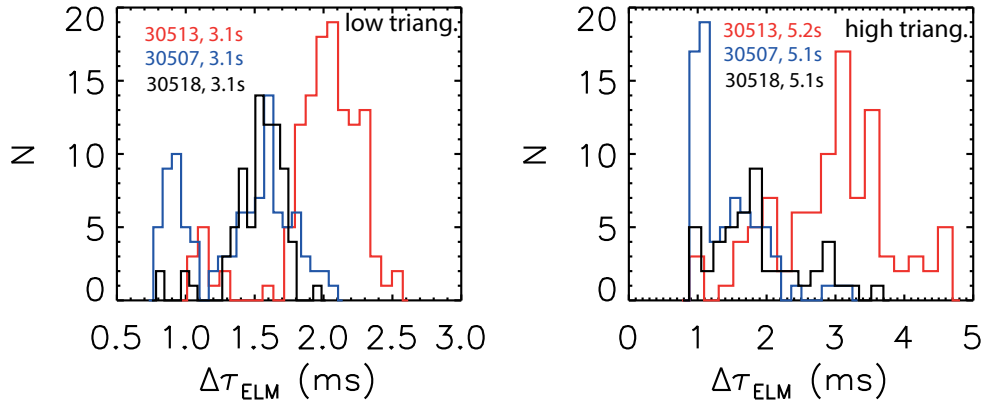

Figure 11: Histogram of ELM collapse times as determined from the width of the ELM peaks of divertor shunt current measurements, same method as in [15], for a) low(3-3.2s) and b) high (5-5.2s) triangularity plasmas.

Section 5: Discussion and conclusions

It is observed in a direct comparison of three plasmas with and without light impurity seeding, that seeding either nitrogen or carbon can lead to a similar increase of the pedestal temperature by ~20-30%, in the cases presented here. In combination with core profile stiffness this leads to the same increase in total stored energy. In other aspects the N_2 and CD_4 seeded plasmas are also very similar;

   a) the radiation intensity and location
   b) the effect on divertor detachment state
   c) and the ELMs collapse time is reduced

An orthogonal effect is seen by changing the upper triangularity from $\delta_{up}\sim0.05$ to $\delta_{up}\sim0.3$ (lower triangularity fixed at $\delta_{low}\sim0.45$), which increases the plasmas density from $6.5 \times 10^{19} m^{-3}$ to $9 \times 10^{19} m^{-3}$ at constant temperature, in both seeded and unseeded plasmas. In this AUG-W

experiment, no difference is seen on the effect of seeding on pedestal confinement improvement between low and high triangularity plasmas. This is in contrast to observations reported on JET in [9]

The experiment nevertheless show that in a metal wall device where the presence of carbon is disallowed due to tritium retention issues, nitrogen can be used to replace it as a radiator. Moreover it shows that the lower confinement often found in metal devices compared to carbon devices can (at least partly) be recovered by extrinsic nitrogen seeding. The outstanding question remains: What causes this confinement benefit driven by the pedestal temperature increase? Possible physics mechanisms have been studied in literature, but none give a conclusive answer.

Ion dilution: The confinement benefit cannot stem from a dilution effect in combination with a hollow Z_{eff} profile. Although . Figure 4 indeed shows that the Z_{eff} profile is slightly hollow, this is insufficient to lead to a 20-30% confinement increase, as quantified in [6]. In order to obtain a confinement benefit a strongly hollow Z_{eff} profile is required that shows a strong rise around the pedestal region. Figure 4 however shows that instead that Z_{eff} features a decrease in pedestal region and approaches unity at the separatrix.

Core transport: The core profiles are stiff, as shown in [5,6,7,16] so the confinement benefit cannot be caused by reduced core transport.

Reduced particle exhaust: both carbon and nitrogen are 'sticking' impurities [17], and could therefore influence the outgassing of deuterium from the first wall. However no evidence of a reduced neutral particle density is observed, which could have had a beneficial effect on confinement due to reduced pedestal cooling.

Pedestal stability: The seeded and unseeded pedestals are consistent with peeling-ballooning pedestal stability [5]. This as such does not explain why a higher pedestal temperature is obtained. The seeded plasmas have a higher β_N than the unseeded one, which allows for reaching the ballooning limit at elevated pressure gradient. However, this does not explain the dynamics how the plasma reaches the increased β_N in the first place

Another related possibility is that the impurity seeding affects the ratio of pressure gradient versus bootstrap current [7] in a way that allows a route to larger pressure gradients. This indeed can happen, but pedestal modelling shows that this can only cover a ~5% increase in p_{ped} in a static situation [7].

Separatrix temperature: Finally, an option is presented where N_2 (or CD_4) seeding cools the separatrix temperature which effectively then shifts the steep pressure gradient region inwards to a region in the magnetic equilibrium where increased pressure gradients can be sustained. Simulations for JET have shown that a reduction of T_{sep} from 100eV to 80eV, combined with a rigid shift of a modelled tangent hyperbolic pedestal profile, can indeed lead to an increase of the pedestal top pressure by 20-30% [18]. This would also require a reduction of the separatrix density, and therefore it is not certain that this is what happens in experiment presented here. The difficulty here is that to verify this mechanism experimentally, the profiles position with respect to the magnetic equilibrium needs to be known well within the current error margin of ~1cm.

In conclusion, the experiment presented here, comparing only three plasmas, show that seeding N_2 and CD_4 can lead to very similar beneficial effect on plasma confinement. More extensive experiments are required to show the effect on confinement of seeding either N_2 or CD_4 in a wider range of plasmas conditions, such as e.g. the influence of normalised pressure, fuelling and seeding levels etc. Nevertheless, the low Z impurity concentration is similar (1-2%), in the experiment discussed, to that observed in carbon devices. It can therefore be implied that in carbon devices the intrinsic carbon has a similarly beneficial effect on confinement to CD_4 seeding in metal devices. Therefore it is likely that the effect of intrinsic carbon, can (at least in the case presented here) be substituted by nitrogen in metal devices. The two gases have very similar radiation potential and as Figure 5 shows, radiate mostly at temperatures below $T_e=100eV$. This means that they have the potential to cool the separatrix (with $T_e < 100eV$) without significant radiation inside the separatrix (with $T_e > 100eV$), which could potentially deteriorate the pedestal.

However, it remains an open question whether nitrogen is allowed as a seeding gas in future fusion reactors due to its tritium handling compatibility. Therefore alternative seeding gasses need to be explored. As a comparison, Figure 5 shows the radiation potential of Ne and Ar as potential seeding gasses. With seeding these two gasses so far no pedestal confinement improvement has been observed in metal devices [e.g 9 for Neon], be it that the documentation in literature is scarce. Both gasses have significant radiation potential above a temperature of 100eV (Figure 5), and could possibly through radiation inside the separatrix deteriorate the pedestal confinement, and possibly cancel any other beneficial effects of the presence of these light impurities in the pedestal region. Therefore, experiments in 2016 will aim at a detailed comparison of the effect of argon, neon, nitrogen and carbon seeding on the (pedestal) confinement.

Ackowledgements

References

[1] A. Kallenbach, et al. Plasma Physics and Controlled Fusion, 55(12), 2013.
[2] A. Kallenbach et al 2015 Nucl. Fusion 55 053026
[3] F. Reimold et al 2015 Nucl. Fusion 55 033004
[4] J. Schweinzer, et al. Nuclear Fusion, 51(11), 2011
[5] C. Giroud et al. Nuclear Fusion, 53(11), 2013
[6] M. Beurskens et al Plasma Phys. Control. Fusion 55 (2013)
[7] M. Dunne et al. In 42nd EPS Conference on Plasma Physics, Lisbon, 2015.
[8] C. Giroud et al, Nucl. Fusion 52 (2012) 063022
[9] C. Giroud et al. Plasma Phys. Control. Fusion 57 (2015) 035004
[10] T. Pütterich et al., Journal of Nuclear Materials 415 (2011) S334–S339
[11] Summers, H. P., ADAS User Manual, 2nd edition, version 2.7 (2004).
[12] P. Stangeby, ISBN 0750305592, IoP Publishing, 2000, book title: "The Plasma Boundary of Magnetic Fusion Devices"
[13] P Snyder et al Nucl. Fusion 51 (2011) 103016 (8pp)
[14] P. Schneider et al, Plasma Phys. Control. Fusion, 56 2014

[15] L Frassinetti et al. Nucl. Fusion 55 (2015)
[16] G. Tardini et al, 2013 Plasma Phys. Control. Fusion 55 015010
[17] S Brezinszek et al, Journal of Nuclear Mat. 2014
[18] S Saarelma et al, Physics of Plasmas 2015